RESEARCH ARTICLE

A Conformal Leaky-Wave Antenna Design for IoMT-Based WBANs

NASSER MONTASERI[1,2]**, ZEYNAB KHODKAR**[3]**, JAMSHID ABOUEI**[4]**, (Senior Member, IEEE),**
WILLIAM G. WHITTOW[5]**, (Senior Member, IEEE), AND**
KONSTANTINOS N. PLATANIOTIS[6]**, (Fellow, IEEE)**

[1]Iran Telecommunication Research Center (ITRC), Tehran 14399-55471, Iran
[2]Department of Electrical and Electronic Engineering, Shahed University, Tehran 33191-18651, Iran
[3]Delta Innovation Center, Iran University of Science and Technology, Tehran 16846-13114, Iran
[4]Department of Electrical Engineering, Yazd University, Yazd 89158-18411, Iran
[5]Wolfson School of Mechanical, Electrical and Manufacturing Engineering, Loughborough University, LE11 3TU Loughborough, U.K.
[6]Department of Electrical and Computer Engineering, University of Toronto, Toronto, ON M5S 1A1, Canada

Corresponding author: Jamshid Abouei (abouei@yazd.ac.ir)

ABSTRACT Continuous health monitoring of vital signs of patients is a challenging issue, especially in emergency medical conditions. This paper designs a practical internet of medical things-based wireless body area network (IoMT-based WBAN), to address this issue. Accordingly, a two-fold test-bed design is proposed taking *i*) signaling and *ii*) antenna configuration into account to attain uninterruptible on/off-body communication links. Firstly, the Walsh-Hadamard coding technique is used in all bio-sensors to retain orthogonal simultaneous signaling for on-body links. Secondly, an antenna configuration of the hub is designed so that it prevents probable interruptions in off-body links which may be caused by some human postures. More accurately, a novel periodic leaky-wave antenna (LWA) with an elliptical belt shape is introduced which generates a quasi-omnidirectional pattern. The LWA is designed based on a multi-tone periodicity of a width-modulated microstrip line. At the design frequency of 5.8 GHz, the suggested conformal periodic LWA was simulated and then fabricated. Simulations and measurement results illustrate that the performance of on/off-body communication links is improved in comparison to conventional antennas. Furthermore, simulated and measured radiation patterns have a good agreement with theoretical calculations. Moreover, specific absorption rate (SAR) values of the proposed antenna are significantly below the SAR limits so that this technique can be highly recommended for WBAN applications.

INDEX TERMS IoMT-based WBAN, continues health monitoring, conformal array, multi-tone periodicity, periodic LWA, open stopband.

I. INTRODUCTION

Internet of medical things-based wireless body-area network (IoMT-based WBAN), a promising technology in continuously patient tracking and health monitoring applications, has recently received considerable attention, even in 5G and beyond 6G systems [1], [2], [3], [4], [5]. The IEEE Std 802.15.6-2012 is the published international standard for WBAN, based on which various frequency bands are

allocated to WBAN applications, such as 402–405 MHz medical implant communication services band, 902–928; 2400–2500; 5725–5875 MHz industrial, scientific, and medical (ISM) band, 3.1-10.76 GHz ultra-wideband range [6]. Patients' monitoring is accomplished by the accommodation of several bio-sensors, all of which send vital information to a unit, known a hub, through wireless on-body communication links. The hub can be worn by the patient to collect the aforementioned data and send them to a health monitoring center via an off-body communication link [7]. Obviously, a patient's comfort is an important demand

The associate editor coordinating the review of this manuscript and approving it for publication was Chan Hwang See.

that should be considered in the antenna design procedure. Some specific requirement expected from hub antennas are their lightweight, low profile, and high adaptability to the human body's surface. Besides, wearable antennas provide omnipresent monitoring which is a key requirement for continuously controlling the vital signs of patients who need emergent care. Accordingly, wearable antennas are commonly adopted in the hub design as they properly meet the above mentioned demands.

Several types of wearable antennas have been studied for on/off-body propagation links, including vertical monopoles [8], [9], [10], [11], planar monopoles [12], [13], [14], planar inverted-F antennas [15], microstrip patches [16], [17], [18], [19], cavity-backed slots [20], [21], [22], [23], and artificial magnetic conducting surface backed antennas [24], [25], [26], [27]. Monopole and inverted-F antennas are suitable for on-body propagation links but they are not low profile designs. Although planar monopole and some planar inverted-F antennas have a small size, a huge amount of the energy is propagated into the human body. Microstrip patch and cavity-backed slot antennas have broadside radiation patterns but these types of antennas have narrow frequency bandwidths. Artificial magnetic conducting planes are designed to provide a high level of isolation between the human tissue and the antenna. The main disadvantages of this method are the relatively large profile and frequency shifts caused by bending. Meanwhile, most of the existing antennas are commonly excited by a coaxial probe perpendicular to the human body surface. This leads to a protrusion which is unsuitable for the required low profile structure.

Uninterruptible monitoring of patients is a key factor in properly encountering their emergency medical conditions. Some patients' postures may limit data transmission from the hub to access points. Therefore, designing a wearable antenna for the hub can retain on- or off-body communication links independently to the patient's posture. The hub's antenna with an omnidirectional pattern may be a suitable idea to attain this aim provided that allowable isolation is obtained between the human tissue and the hub's antenna. However, none of the aforementioned antennas can simultaneously satisfy all of these requirements. Hence in this work, it is suggested to utilize a conformal leaky-wave antenna (LWA) based on a metasurface for the hub. LWAs are greatly popular because of their low-profile construction, structural simplicity for the fabrication, and highly directive beams [28]. Recently, various types of LWAs are studied based on sinusoidally modulated structures, which are implemented on planar [29], [30], [31], [32], [33] or conformal configurations [34], [35]. To the best of our knowledge, there is no existing work on employing LWAs in WBAN applications.

Regarding the above-mentioned strategy, off-body communication links continuously exist, independent of the patient's posture. On the other hand, on-body links have to take place in data transmission, without any interruption. To retain on-body links, all bio-sensors should simultaneously transmit vital signs to the hub. In this work, this demand is met by employing an orthogonal signaling using the Walsh-Hadamard coding scheme [36] for on-body links. Thus, bio-sensors can simultaneously communicate with the hub without any data collision. The main novel contributions of this work are listed as follows:

1) A practical IoMT-based WBAN is designed to attain an uninterruptible patient monitoring system. In this regard, *i*) an orthogonal signaling using Walsh-Hadamard coding technique in all bio-sensors, and *ii*) specific antenna characteristics in the hub structure, are proposed for on- and off-body communication links, respectively.

2) A novel conformal LWA is synthesized and designed based on a multi-tone width-modulated microstrip line.

3) The suggested antenna is implemented on a thin flexible substrate that can easily bend around the human abdomen similar to a belt.

4) The proposed antenna provides a quasi-omnidirectional pattern, which leads to an enhancement in the off-body communication link's performance, for practical WBAN applications.

5) The connection between bio-sensors and the proposed antenna will not be restricted to the patient's posture, whereas the conventional hub's antennas might not work when the patient falls on the ground.

6) The isolation between the proposed antenna and the human tissue satisfies safety standards for medical applications, i.e., a SAR value as small as 0.15 W/kg corresponding to the 1 W input power.

This paper is organized as follows: Section II indicates the testbed model of the proposed network, introduces bio-sensors' characteristics, and presents the signaling design of applied sensors based on the Walsh-Hadamard coding technique. In Section III, an elliptical conformal array antenna is designed and synthesized so that a quasi-omnidirectional radiation pattern at the azimuth plane is achieved. In order to realize the proposed conformal array, a modulated metasurface antenna based on leaky-wave concepts is utilized as investigated in Section IV. The proposed LWA has a novel configuration of the multi-periodic width-modulated microstrip line. Simulation, fabrication, and measurement of the proposed LWA are presented in Section V. Finally, the paper is concluded in Section VI.

II. TESTBED MODEL

One of the critical concerns in patient monitoring is to receive the vital signs without any interruption. In order to attain this purpose, the issue is investigated in the paper from two different perspectives: *i*) introducing a conformal antenna design and *ii*) establishing an orthogonal channel coding scheme. Thanks to the proposed antenna structure, the off-body links continuously transmit/receive signals so that the whole antenna would not be blocked if the patient falls on the ground, sleeps on the bed, or has any other posture. Besides, it is required to enable continuous interference-free on-body
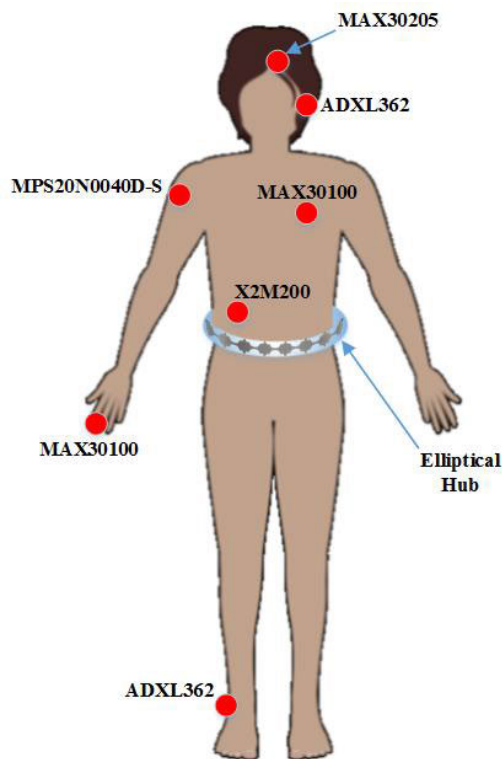
FIGURE 1. The system model of proposed practical IOMT-based WBAN network with the belt-shape hub's antenna and sensors that are labeled by their intended device name as listed in Table. 1.

communication links so that all sensors simultaneously transmit vital data to the hub. The lack of orthogonality in on-body link codes restricts the system design to accommodate a scheduling scheme. Then, only one sensor is allowed to transmit a signal each time slot. Therefore, some vital signs might be lost and, consequently, the patient may be at risk. Hence, Walsh Hadamard (WH) channel coding method is used for the sensors' transmitters. According to the proposed testbed model, the LWA together with the WH scheme maintain continuous communication links.

To get more insight into the application of the designed LWA in healthcare services, consider a practical two-tier IoMT-based WBAN as shown in Fig. 1. The suggested testbed is composed of five bio-sensors, as indicated in Table 1, connected to seven different points on the patient's body and a hub with an elliptical antenna around abdomen of patient. The hub collects data from sensors and transmits them to some static access points. Regarding the emergency conditions of patients, these bio-sensors continuously sense vital signs and simultaneously transmit them to the hub according to the star topology.

The practical pulse shape model of each bio-sensor is shown in Fig. 2(a), where three operational sleep, transition, and active states are indicated in detail. During the sleep state, sensors neither transmit nor receive any data. It should be noted that the combination of transmission and receive states is commonly known as active mode. Indeed, any data

exchange between sensors and hub only occurs in the active mode. Therefore, they are merged together for simplicity. Finally, the transition mode indicates that the operational state of a sensor is changing from a state to another. Subsequently, possible collisions may happen when multiple sensors simultaneously meet TX/RX operational state. In order to explain this phenomenon more precisely, the duty cycle of all five sensors has been shown in Fig. 2(b) based on their individual sensing frequencies, introduced in Table 1. Note that various sensors have different sensing frequencies and no interruption is permitted for vital sensors' operation. However, as it can be seen from Fig. 2(b), some time slots may suffer from possible collisions, such as 51, 55, 251, 253, and 4999 ms, where some sensors simultaneously meet the active mode. In fact, independent of the starting point's mode, the occurrence of disruptive collision in some time slots is unavoidable.

Among various multiple access techniques, the orthogonal signaling using code division multiple access technique is the best choice that allows all sensors to continuously operate and simultaneously experience the active mode. Accordingly, Walsh-Hadamard (WH) coding technique is employed to prevent any collision and increase the energy efficiency of the network. In this regard, each bio-sensor multiplies its intended transmit data to a code achieved from a row of square $N \times N$ WH matrix, denoted by $\mathbf{H}_{2^k}$, $k = 0, 1, 2, \ldots$, leading to mutual orthogonality of data transmitted by multiple bio-sensors. Defining the first dimension as $\mathbf{H}_1 = [1]$, higher dimensions are obtained using the Kronecker product of $\mathbf{H}_{2^k}$ to $\mathbf{H}_{2^{k-1}}$ as

$$\mathbf{H}_{2^k} = \mathbf{H}_2 \otimes \mathbf{H}_{2^{k-1}} = \begin{bmatrix} \mathbf{H}_{2^{k-1}} & \mathbf{H}_{2^{k-1}} \\ \mathbf{H}_{2^{k-1}} & -\mathbf{H}_{2^{k-1}} \end{bmatrix}. \quad (1)$$

In the zero-phase, generated codes are mutually orthogonal as the cross-correlation of each pair rows of WH matrix is zero, which may not hold for non-zero phase shifts. To tackle this issue and ensure the orthogonality of codes in all phase shifts $\theta = 0, \ldots, 2^k - 1$, $k+1$ special codes are extracted from $\mathbf{H}_{2^k}$ [36]. Based on this, the orthogonality of codes does not depend on phase shifts, no longer, leading to the avoidance of any inter-channel interference. Therefore in our testbed, where seven on-body bio-sensors simultaneously send data, orthogonal codes in every $\theta = 0, 1, \ldots, 2^6 - 1$ phase shift are generated from $\mathbf{H}_{2^6}$ WH matrix. Let define the set of 2^6 codes generated from the WH matrix $\mathbf{H}_{2^6}$ as $\mathbf{C}\left(2^6, 6\right)$. Then, the cross-correlation for each arbitrary pair of codes $c_i, c_j \in \mathbf{C}\left(2^6, 6\right)$, $i \neq j$, at phase shift θ is calculated as

$$R_{c_i c_j}(\theta) = \sum_{n=1}^{2^6} c_i(n) c_j(n + \theta) \quad (2)$$

which is expected to be zero for all values of $\theta = 0, \ldots, 2^6 - 1$. As mentioned before, a set of $K = k + 1 = 7$ codes is extracted from $\mathbf{C}\left(2^6, 6\right)$ to prevent the non-orthogonality of codes, caused by probable phase shifts. Hence, it can be used for transmissions of sensors in the proposed WBAN testbed, to guarantee that data exchange is collision-free and reliable.

TABLE 1. Some specific features of bio-sensors, including their industrial name, applications, frequencies, and power characteristics.

| Device ID	Application	Connection location	Sensing Frequency	Power Consumption	Power Supply
MAX30100	Pulse Oximeter ECG	Finger Tip Left Side of Chest	500 Hz	464 mW	1.8-3.3 V
MAX30205	Body TMP	Forehead	0.2 Hz	1951 mW	2.7-3.3 V
ADXL362	Accelerometer Hearing Aids	Wrist/Arm/Ankle Ear	12.5-400 Hz	5 μW	1.6-3.5 V
MPS20N0040D-S	Blood Pressure	Arm	4 Hz	-	5 V
X2M200	Respiration Rate	Abdomen	20 Hz	435 mW	3.3-5.5 V
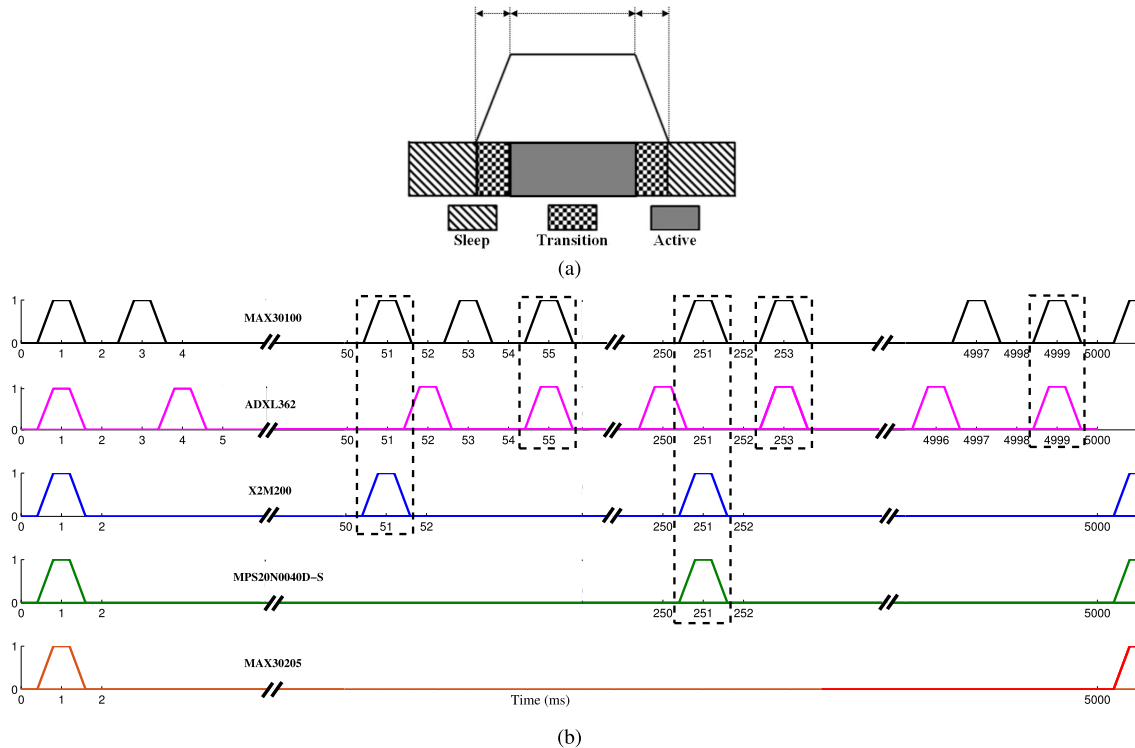
FIGURE 2. a) The power profile of a typical pulse shape of bio-sensors and related three operational states, b) Duty cycles of applied bio-sensors and exhibition of probable overlaps of pulses during active mode.

III. CONFORMAL ARRAY ANTENNA DESIGN

As previously mentioned, it is required to design a specific antenna with an omnidirectional pattern at the azimuth plane in the ISM band (5725–5875 MHz) for both on- and off-body WBAN links. Besides, the intended antenna must achieve an average SAR value below 1.6 W/kg over 1 g of tissue according to the IEEE *C*95 standard [37]. In Table 2, some types of conventional antennas which are able to produce omnidirectional patterns are investigated. Although planar and/or vertical monopole antennas can produce an ideal omnidirectional pattern, a significant amount of radiated power absorbed in the human body leads to high SAR values. Therefore, these antennas have been utilized for on-body links with a low enough excited power so that the SAR value is acceptable. On the other hand, conformal array antennas can produce the omnidirectional pattern. As an example, the omnidirectional pattern and the acceptable SAR value would be feasible if a conformal phased-array antenna is used around the abdomen. However, this method is expensive, difficult to implement, and would be large. Besides, thin microstrip arrays with flexible structures around the body's abdomen

may be good choices for this purpose. For instance, corporate- or series-fed microstrip arrays [38], [39], [40] can synthesize the arbitrary pattern and provide a low-level SAR. The main limiting factors in corporate- and series-fed methods are the antenna's width and expected frequency bandwidth, respectively. Actually, the proposed on- and off-body WBAN models need an antenna with a flexible structure, wide frequency bandwidth, omnidirectional pattern, low-cost fabrication, low profile, simple construction, lightweight, and an acceptable SAR value. To meet all of these demands, we propose an LWA based on a multiperiodic width-modulated microstrip line so that a quasi-omnidirectional pattern and an acceptable SAR value are provided. The designed antenna is flexible enough so that it is wearable as a belt around the abdomen of the human body.

A. PROPOSED ARRAY CONFIGURATION

A heuristic conformal array antenna is proposed with an elliptical shape. The periphery of the ellipse is assumed to be 96 cm for a male volunteer with age-35 y, mass-80 kg, and height-180 cm. Elliptic major and minor diameters are about

TABLE 2. Qualitative comparison between various common antennas to produce omni or quasi-omni directional patterns.

Structure	Antenna type	Δf	Pattern	Cost	Size	Implementation	SAR
Planar	Monopole	Wide ✓	Omni ✓	Cheap ✓	Very small ✓	Easy ✓	High ×
Conformal	Phased-array	Moderate ✓	Omni ✓	Expensive ×	Large ×	Difficult ×	Low ✓
	Series-fed MA	Narrow ×	Quasi-omni ✓	Cheap ✓	Small ✓	Easy ✓	Low ✓
	Corporate-fed MA	Narrow ×	Omni ✓	Cheap ✓	Large ×	Easy ✓	Low ✓
	Proposed LWA	Wide ✓	Quasi-omni ✓	Cheap ✓	Small ✓	Easy ✓	Low ✓

MA and Δf represent microstrip array and frequency bandwidth, respectively.
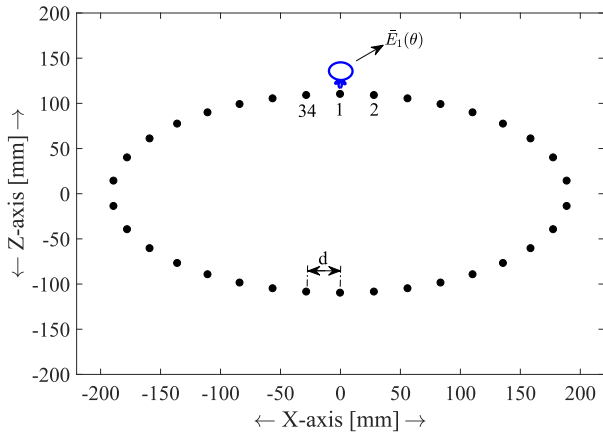

FIGURE 3. Conformal array antenna including *N* = 34 elements around the ellipse in the *X* − *Z* plane, where *d* represents the distance between elements.

381 mm and 220 mm, respectively. For this configuration, the distance between elements is obtained as $d \simeq \lambda_g/2 \simeq 28.2$ mm, where λ_g is the wavelength of the microstrip line, and this allows to have *N* = 34 elements around the ellipse. Fig. 3 illustrates the arrangement of such array elements in the *X* − *Z* plane.

To achieve an omnidirectional pattern in the *X* − *Z* plane, elements are supposed to be excited with equal phase and nonuniform amplitude. Therefore, the corresponding far-field expression for this array in the *X* − *Z* plane is given by:

$$\bar{E}(\theta) = \sum_{n=1}^{N} V_n \bar{E}_n(\theta) \, e^{jk_0[x_n \sin\theta + z_n \cos\theta]}, \qquad (3)$$

where V_n is the amplitude of nth element, k_0 represents the free-space wavenumber, and $\bar{E}_n(\theta)$ denotes the pattern of nth element, which is a function of the element's position, as well. To approximately realize an omnidirectional pattern, it is required to optimize V_n, provided that the element factor is known. For such a configuration, the error function is calculated as

$$Error = 1 - \int_{-\pi}^{\pi} \frac{\bar{E}_{norm}(\theta)}{2\pi} \, d\theta, \qquad (4)$$

in which $\bar{E}_{norm}$ is the normalized radiation pattern. Obviously in omnidirectional patterns, the radiation pattern in the *X* − *Z* plane is $\bar{E}_{norm}(\theta) = 1$, which leads to *Error* = 0. In this work, it is supposed that array elements merely radiate toward the

outside of the ellipse with radiation patterns as follows:

$$\bar{E}_n(\theta) = \begin{cases} \sqrt{\cos(\theta - \theta_n)} & |\theta| \leq \pi/2 \\ 0 & \text{otherwise,} \end{cases} \qquad (5)$$

where θ_n denotes the local direction of nth pattern. There are several optimization methods to design and synthesis an array antenna for the desired radiation pattern such as genetic algorithm (GA), particle swarm optimization, and invasive weed optimization [41], [42]. In this work, the amplitude of the array antenna is optimized using GA so that a minimum ripple is observed in the radiation pattern, whose behavior is similar to the omnidirectional pattern. Due to the symmetrical shape of the proposed array, only a few elements are employed in the optimization procedure, i.e., $n \in \{1, \ldots, 9\}$, and the results are considered for remaining elements, as well. The obtained results from the GA optimization including the normalized amplitude coefficients V_ns versus the elements' number are shown in Fig. 4. The elliptical array with these amplitude coefficients and the same excited phases has a quasi-omnidirectional pattern. The radiation pattern corresponding to this conformal array will be depicted and evaluated in Section V. As will be seen in Section V, the radiation pattern obtained by a theoretical calculation has an omnidirectional behavior with a 2.5 dBi ripple in the gain. It should be noted that when an antenna is designed with different periphery values, the number of elements should be calculated first. Secondly, as mentioned above, the amplitude's elements should be obtained using optimization methods, such a GA.

B. FROM THEORETICAL CONFORMAL ARRAY TO REALIZABLE LWA

In the previous subsection, an elliptical array was designed with nonuniform excitation amplitudes V_ns of the elements which have the same phase excitation. Regarding the above-mentioned strategy, the proposed off-body WBAN model needs an antenna with a flexible structure, low profile frame, high radiation efficiency, and wide frequency bandwidth. To reach all of these requirements, we focus our attention on an LWA based on a thin flexible substrate. In periodic LWAs with period *d* along the *Z*–axis, the wavenumber contains an infinite number of space harmonics (Floquet harmonics) represented as [28]:

$$k_{z_n} = \beta_n - j\alpha = \beta_0 - j\alpha + \frac{2n\pi}{d}, \qquad (6)$$

where β_0 represents the fundamental phase (propagation) constant, α denotes the attenuation (leakage) constant, and
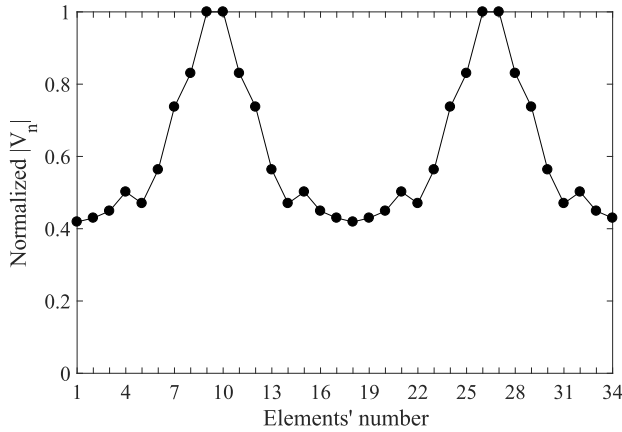
FIGURE 4. The normalized elements' amplitude of the conformal elliptical array versus the elements' number to achieve an omnidirectional pattern with the minimum ripple using the GA optimization method.

FIGURE 5. The theoretical calculation of normalized leakage constant along the LWA as a function of z/λ_0 with the distribution of field's amplitude illustrated in Fig. 4.

n is an integer. The fundamental space harmonic with the wavenumber $k_{z_0} = \kappa = \beta_0 - j\alpha$ is usually a slow wave ($\beta_0 > k_0$). Besides, a leakage and, consequently, radiation will occur from fast space harmonics. As usual, periodic LWAs are designed so that the $n = -1$ space harmonic with $|\beta_{-1}| < k_0$ is the one that is radiated.

In LWAs, the radiation power depends on the attenuation constant, α, along the antenna. For an LWA along the Z–axis, the aperture distribution is expressed as $A(z)e^{-j(k_{z_n})z}$, where $A(z)$ denotes the amplitude of fields. Provided that $A(z)$ is known, the attenuation constant can be obtained as follows [28]:

$$\alpha(z) = \frac{1}{2} \frac{A^2(z)}{(1/\eta) \int_0^L A^2(z)\, dz - \int_0^z A^2(z')\, dz'}, \quad (7)$$

where L is the antenna length and η denotes the radiation efficiency, which usually is assumed 90% in LWAs. The leakage constant along the LWA is obtained by substituting the calculated elements' amplitude extracted from Fig. 4 into Eq. (7). Fig. 5 illustrates the normalized leakage constant along the considered LWA as a function of z/λ_0, where λ_0 denotes the free-space wavelength and the antenna's length is about $L = 18.56\lambda_0 \simeq 96$ cm.

IV. LEAKY-WAVE ANTENNA (LWA) IMPLEMENTATION

Since elements of the designed array have equal excitation phase values, the leaky-wave structure must radiate in the broadside region where the 2nd stopband, known as open stopband, occurs [28]. Therefore, it is required to design a periodic LWA with broadside radiation capability. In periodic LWAs, achieving broadside radiation is difficult because an open stopband occurs. Since the leakage constant varies rapidly in the open stopband region, a large amount of power is reflected back to the source. Thus, the radiation power drops substantially. To mitigate or suppress the open stopband effect, several techniques have been proposed, such as reflection-canceling [43], implementing asymmetric unit
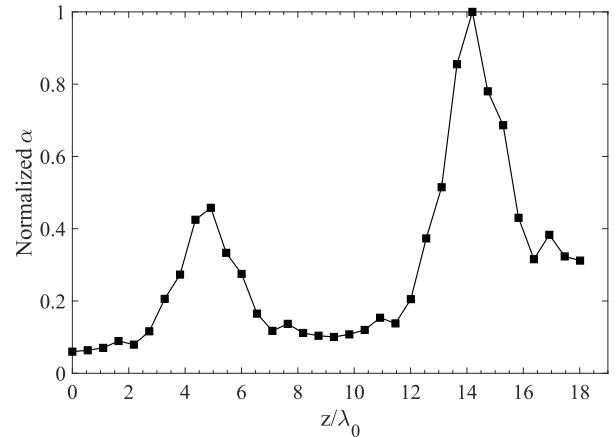
structure [44], impedance-matching [45], [46], and multi-tone periodicity [47]. In this work, we design a periodic LWA based on the width-modulated microstrip line. In order to suppress the open stopband effect, a multi-tone periodicity technique is employed which utilizes several modulation indices.

A. MODULATED DIELECTRIC MEDIA

Let's consider a modulated dielectric medium with the effective permittivity, ε_e, defined as follows [48]:

$$\varepsilon_e = \varepsilon_0 \varepsilon_r = \varepsilon_0 \varepsilon_{avg} \left\{ 1 + \sum_{n=1}^{\infty} M_n \cos\left(\frac{2n\pi}{d}z\right) \right\}, \quad (8)$$

where d is the periodicity, M_n are known modulation indices, ε_0 represents the free-space permittivity, ε_{e_r} and ε_{avg} denote effective and average dielectric constants, respectively. In this medium, the wave equation of transverse magnetic (TM) mode is in a general form of the Hill's equation [48], [49], [50], which is briefly described in Appendix A. Once the Hill equation is solved, κ and k_{z_n} are obtained, wherein real and complex values of κ are the so-called "stable" and "unstable solutions" of the Hill equation, respectively. To consider this medium, the relation between κ, k_0, d, M_n, and ε_{avg} can be investigated in the well-known form of the "stability chart".

As an example, Fig. 6 depicts the stability chart of the Hill equation with parameters $\theta_2 = 0.75\theta_1$, $\theta_3 = -\theta_1$, $\theta_5 = 2.5\theta_1$, $\theta_7 = -5\theta_1$, and $\theta_n = 0$ (n is a non-negative integer and $n \notin \{0, 1, 2, 3, 5, 7\}$), where shaded and unshaded zones are stable and unstable regions, respectively. Relying on the stability chart, the 1st and 2nd stopbands occur around $\theta_0 = 1$ and 4, respectively. As seen from Fig. 6, the straight line $\theta_1 = 0.3312\theta_0$ passes through the stable and unstable regions. Obviously along this straight line, the 2nd stopband's width in the vicinity of $\theta_0 = 3.503$ is eliminated. We call this point with the coordinate $[\theta_0, \theta_1] = [3.503, 1.16]$ as the "stable point". As expected, if $\theta_3 = -\theta_1$, $\theta_5 = 2.5\theta_1$, and $\theta_7 = -5\theta_1$ are fixed and θ_2 is changed, the stable point would
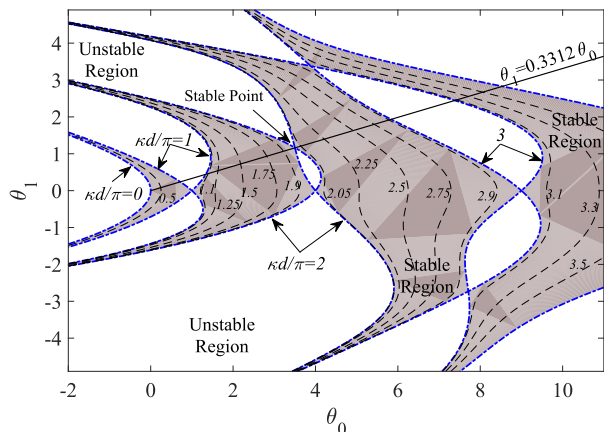
FIGURE 6. The stability chart of the Hill equation, where $\theta_2 = 0.75\theta_1$, $\theta_3 = -\theta_1$, $\theta_5 = 2.5\theta_1$, and $\theta_7 = -5\theta_1$.

FIGURE 7. The microstrip line width *W* versus the effective dielectric constant ε_{e_r} at 5.8 GHz.

FIGURE 8. Unit cells of the multi-tone width-modulated microstrip line corresponding to dielectric media with a) $\theta_2 = 0.075\theta_1$ and b) $\theta_2 = 0.035\theta_1$.

be displaced which leads to alternation of the straight line's slope.

In the stability chart for the transverse electric (TE) mode, the slope of the straight line $\theta_1 = m'\theta_0$ is directly proportional to the modulation index M_1, i.e., $m' = 0.5M_1$. Similarly in the TM mode, m' depends on M_1 and other modulation indices. Besides, the stable point and, consequently, m' can be tuned by choosing different values of θ_2. Therefore, it is possible to control modulation indices, specifically M_1, so that the 2nd stopband is approximately suppressed. It should be noted that θ_ns depend on parameters of the dielectric medium, such as M_n, k_0, d, and ε_{avg} (see [48] and Appendix A). Regarding a large number of θ_n indices in the Hill equation, there exist considerable degrees of freedom to suppress the 2nd stopband. In the calculation procedure of θ_n indices, it is essentially important to utilize an appropriate value of θ_n so that the desired periodic LWA would be realizable based on the width-modulated microstrip line. In this work, θ_2 is selected between $0.03\theta_1$ and $0.085\theta_1$ in 16 states and the corresponding modulation indices are numerically calculated. For example, using numerical calculation, the corresponding parameters of dielectric medium with coefficients $\theta_2 = 0.075\theta_1$, $\theta_3 = -\theta_1$, $\theta_5 = 2.5\theta_1$, and $\theta_7 = -5\theta_1$ are approximately calculated as $k_0d/\pi = 1.1368$, $\varepsilon_{avg} = 3.1115$, $M_1 \simeq 0.11737$, $M_2 \simeq -0.028715$, $M_3 \simeq 0.010651$, $M_4 \simeq 0.000931$, $M_5 \simeq -0.012159$, $M_6 \simeq 0.0001033$, $M_7 \simeq 0.012019$, $M_8 \simeq 0.0004879$, $M_9 \simeq 0.000159$, and $M_n \simeq 0$ ($\forall n \geq 10$).

B. UNIT CELL DESIGN

Recently, relying on the theoretical concept of electromagnetic wave propagation along modulated dielectric media, new planar LWAs have been proposed [51], [52]. In this method, a periodic medium is implemented using a width-modulated microstrip line. In this work, we follow this method and design a leaky-wave surface with arbitrary modulation indices. The effective dielectric constant of a microstrip
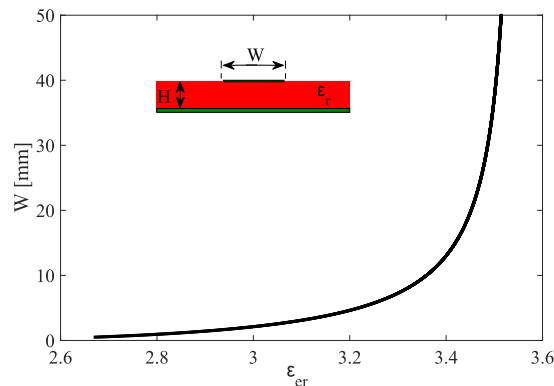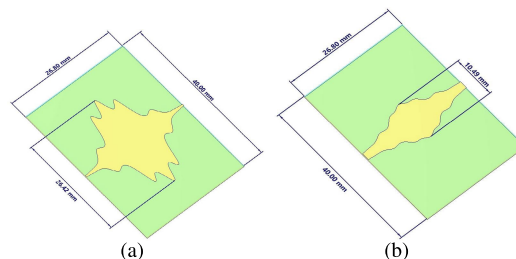
line at the frequency f can be obtained as

$$\varepsilon_{e_r}(f) = \varepsilon_r - \frac{\varepsilon_r - \varepsilon_{e_r}(0)}{1 + (f/f_{50})^m}, \qquad (9)$$

where $\varepsilon_{e_r}(0)$ denotes the effective dielectric constant at the zero frequency and parameters f_{50} and m are given by long expressions presented in [53]. Fig. 7 shows the microstrip line width, W, versus the effective dielectric constant, ε_{e_r}, at 5.8 GHz belonging to the WBAN ISM band, where the grounded dielectric substrate is RO4003 with $\varepsilon_r = 3.55$, $H = 0.508$ mm, and $\tan\delta = 0.0027$. For a variation of the microstrip line width between 0.5 and 40 mm, ε_{e_r} is obtained between 2.7 and 3.5, respectively.

In the previous subsection, modulated dielectric media are designed for 16 types of θ_n. In this subsection, these modulated dielectric media are implemented using width-modulated microstrip line. In Fig. 8, two designed unit cells based on the multi-tone width-modulated microstrip line are shown, where $\theta_2 = 0.075\theta_1, 0.035\theta_1$. The corresponding modulation index M_1 for Figs. 8(a) and 8(b) is numerically calculated as 0.056 and 0.117, respectively. It should be noted that the other modulation indices are numerically calculated.

Fig. 9 shows the HFSS simulation of the normalized leakage constant α related to the 16 designed unit cells. As expected, the leakage constant can be controlled by selecting a unit cell with an appropriate value of M_1. Besides, in order to design the proposed conformal LWA with a quasi-omnidirectional pattern, electromagnetic fields should be distributed along the antenna with leakage constant similar to Fig. 5.
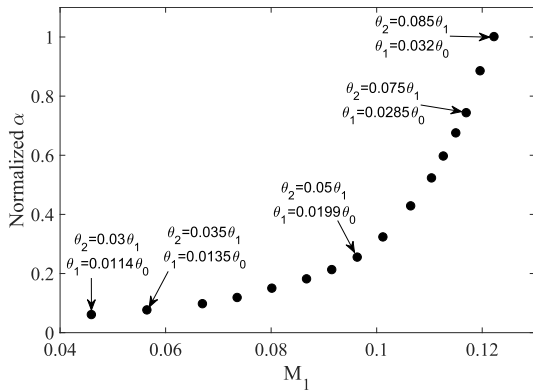
FIGURE 9. Simulation of the normalized leakage constant α versus the modulation index M_1 at 5.8 GHz.

V. SIMULATION, FABRICATION, AND MEASUREMENT

In this section, we present some experimental results of the designed antenna for on- and off-body WBAN applications. Accordingly, a conformal LWA, consisting of 34 unit cells, was designed pursuant to the procedure described in Sections III and IV, such that the radiation pattern of the proposed antenna has a quasi-omnidirectional behavior. Fig. 10(a) shows the fabricated antenna, while the antenna has a flexible form and can be worn as a belt around the human body-abdomen. The fabricated antenna's width and length are 5 and 96 cm, respectively. Both ends of the antenna are connected to 50 Ω SubMiniature version A (SMA) connectors with a feed at one end and a matched load at the other end. Measured and simulated scattering parameters of the designed LWA in the frequency 5.6–6 GHz band are plotted in Fig. 10(b). The fabricated antenna has a good matching performance ($S_{11} < -12.7$ dB) in 5.725–5.875 GHz ISM band. In conventional periodic LWAs, the attenuation constant varies rapidly near the broadside region where the open stopband occurs and, consequently, the input match to the antenna weakens [28]. Fig. 10(b) reveals the absence of input mismatch at the broadside region, vicinity of 5.8 GHz, thanks to the suppression of the open stopband effect described in Section IV(A). Since the fabrication is not accurate enough, and the connectors' loss is not considered in the simulation, measured results have less disparity than simulated results. Nevertheless, there is a good agreement between simulation and measurement results.

A. EVALUATION OF OFF-BODY COMMUNICATION LINK: RADIATION RESULTS

Fig. 11 illustrates the measurement setup of radiation characteristics at the antenna testing lab. To measure the radiation patterns, the fabricated antenna is stuck around an elliptical Teflon structure.

Fig. 12(a) illustrates the simulated 3-D radiation pattern at 5.8 GHz belonging to the WBAN ISM band, where the elliptical LWA is in the $X-Z$ plane. In Fig. 12(b), E-plane radiation patterns in the $X-Z$ plane are shown. There are about 2.5, 3, and 3.5 dB ripples in the theoretical calculated, simulated,
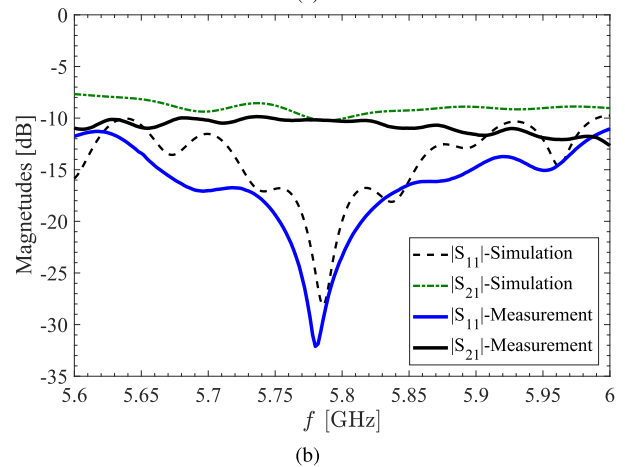

(a)

(b)

FIGURE 10. a) A photograph of the manufactured LWA, b) Simulated and measured S-parameters versus frequency.
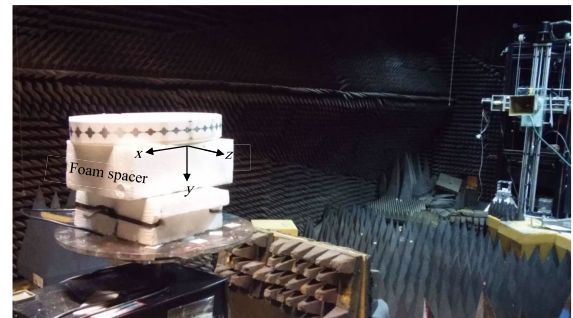

FIGURE 11. The measurement setup of radiation characteristics at the antenna testing Lab.

and measured radiation patterns, respectively. Moreover, simulated and measured cross-polarization levels are less than -20 and -15 dB in the E-plane, respectively. The H-plane radiation patterns in the $Y-Z$ plane are also depicted in Fig. 12(c). In the H-plane, the half-power beam-width is about 68° and 72° for simulated and measured results, respectively. The designed antenna has a realized gain of about 2.5 dBi in simulation and 2 dBi in measurement at 5.8 GHz. Since the antenna is very close to the human body, its performance is evaluated on the phantom model in HFSS simulation. As seen from Fig. 12(b), the E-plane radiation pattern approximately does not change. On the other hand,
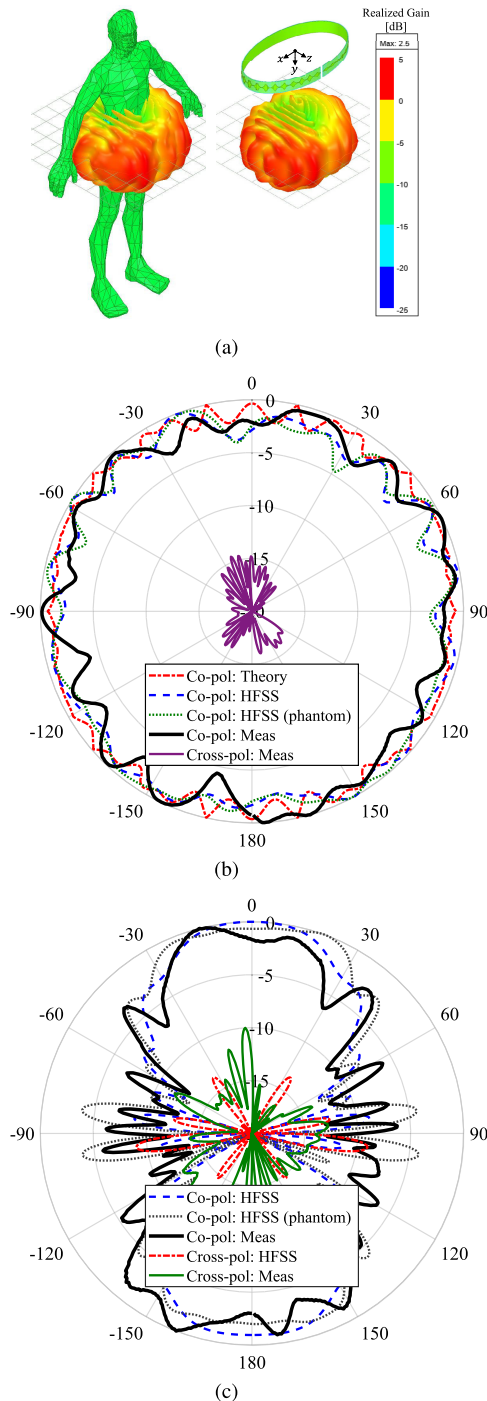
(a)

(b)

(c)

FIGURE 12. Theoretical calculation, simulation, and measurement normalized radiation patterns at the dedicated WBAN ISM frequency of 5.8 GHz, a) simulated 3-D radiation pattern where the antenna is placed on the phantom model or free space, b) E-plane ($X - Z$ plane), and c) H-plane ($Y - Z$ plane).

Fig. 12(c) shows that the H-plane radiation pattern has imperceptibly changed. Therefore, the human body does not considerably affect radiation patterns. Due to the accuracy of the mesh discretization used in HFSS, manufacturing tolerances, and small defects in the measurement process, there is a discrepancy between simulation and measurement results.

Fig. 13 illustrates E-plane radiation patterns at frequencies 5.6, 5.7, 5.9, and 6 GHz. As the frequency moves away from 5.8 GHz, the quasi-omnidirectional behavior of radiation patterns gets worse. In Fig. 14, directivity and realized gain are illustrated versus frequency, where a small drop in directivity and gain has occurred around broadside frequency (5.8 GHz). Moving away from the 5.8 GHz frequency, the radiation pattern tends to a directional form, leading to an increase in the directivity. In fact, this drop is due to the form of radiation pattern but not caused by the broadside stopband. Furthermore, the simulated radiation efficiency of the antenna is illustrated in this figure, which is approximately 80% at the design frequency.

One of the main issues in conventional antennas such as monopoles or patches is that the radiation may be blocked in some patients' postures. For example, if the patient falls on the floor, conventional antennas might be located between the human body and the floor, leading to an interruption in communication. Consequently, the patient may be at risk. Therefore, the off-body communication link between hub and the control center as well as the on-body link between hub and sensors may be disturbed. Since the proposed antenna is wearable like a belt, at least half the antenna length radiates into the free space. Although the radiation efficiency may decrease in this case, the proposed design establishes uninterruptible on/off-body communication links. As an example, Fig. 15(a) shows the simulated 3-D radiation pattern of the LWA which is bent around the human's abdomen. The patient is supposed to be lying on the ground (e.g., soil with parameters of $\varepsilon_{soil} = 12$, $\mu_{soil} = 1$, $tan\delta_{soil} = 0.43$). As seen from this figure, it is obvious that the proposed LWA can radiate into free space. Fig. 15(b) depicts the directivity and realized gain in the E-plane ($X - Z$ plane), where the maximum values are around 10.7 and 2.8 dBi, respectively. In fact, even when the patient is lying on the ground, the LWA can radiate into free space with the total efficiency of about 16.2 %. In this situation, when the wave propagates along the antenna, a portion of the energy comes back to the source due to the mismatch between the antenna and soil. In a region where the antenna is directly connected to the soil, part of the energy penetrates into the soil and the remaining propagates similar to the parallel plate waveguide along the substrate and eventually radiates from remaining parts of the antenna. Thanks to this characteristic on- and off-body communication links would not be interrupted when the patient falls on the ground, in contrast to conventional antennas.

Fig. 16(a) depicts the simulated 3-D radiation pattern of the proposed LWA while the patient is sitting on the chair made of a polyester material with parameters of $\varepsilon_{pol} = 3.2$, $\mu_{pol} = 1$, $tan\delta_{pol} = 0.03$. In Fig. 16(b), the directivity and realized gain in the E-plane ($X - Z$ plane) are shown, where the maximum values are around 6.5 and 3 dBi, respectively. Although the simulated radiation pattern has some nulls, it is still far away from directional form, tending to quasi-omnidirectional pattern. In comparison to previously published where the antenna is located on the back of the patient's body [16],
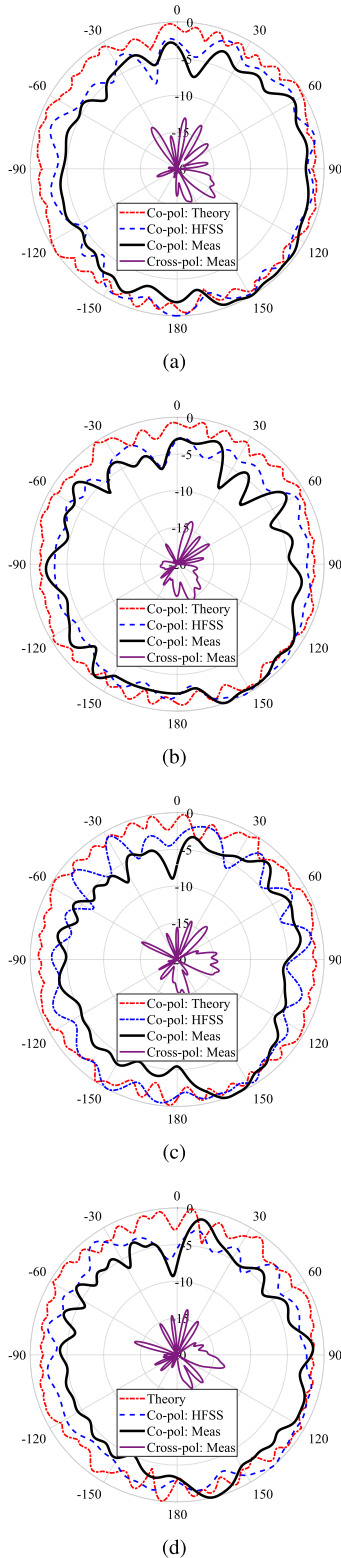
(a)

(b)

(c)

(d)

FIGURE 13. Theoretical calculation, simulation, and measurement E-plane ($X - Z$ plane) normalized radiation patterns at different frequencies: a) 5.6, b) 5.7, c) 5.9, and d) 6 GHz, where the proposed antenna is positioned in $X - Z$ plane as shown in Fig. 11.

[54], the proposed antenna cannot be blocked by the chair or sofa, and a portion of the antenna length can radiate with the tolerable radiation efficiency into free space.
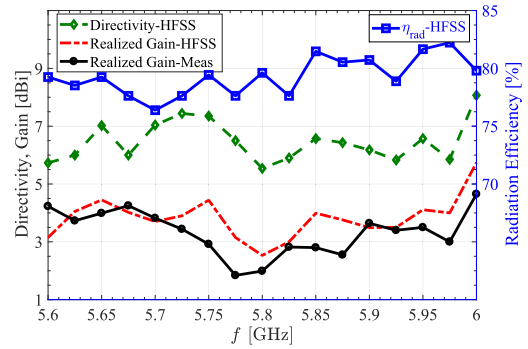

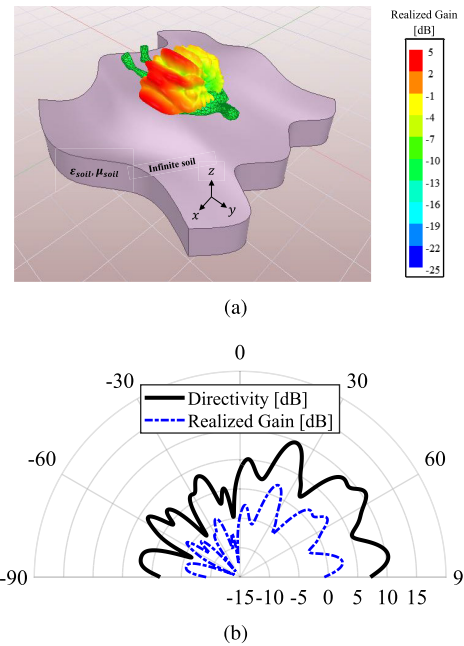**FIGURE 14.** Simulated radiation efficiency, directivity, and realized gain versus frequency.

(a)

(b)

FIGURE 15. Simulated results of antenna's performance while the patient is lying down on the infinite ground (soil) with parameters of $\varepsilon_{soil} = 12$, $\mu_{soil} = 1$, $tan\delta_{soil} = 0.43$; a) 3-D radiation pattern and b) E-plane ($X - Z$ plane) patterns at the frequency of 5.8 GHz.

B. EVALUATION OF ON-BODY COMMUNICATION LINK: PATH LOSS BETWEEN HUB (LWA) AND SENSORS

On-body links between the hub and sensors are shown in Fig. 1. The sensor nodes transmit the vital data to hub, then, the hub is connected to the control center via off-body links. In conventional systems, sensors are composed of some ultra-wideband (UWB) antennas with an omnidirectional pattern. On the other hand, the conventional hub is equipped with an antenna which has a directional pattern. Since the sensor nodes are often energy-constrained [55], the evaluation of path loss between sensors and hub should be considered in on-body communication links. As shown in figures 17(a) and (b), wideband monopole and microstrip patch antennas with detailed dimensions were designed and fabricated with omnidirectional and directional patterns, respectively. During the test procedure, the fabricated monopole and patch antennas are used as the sensor and conventional hub, respectively. Both of the antennas are
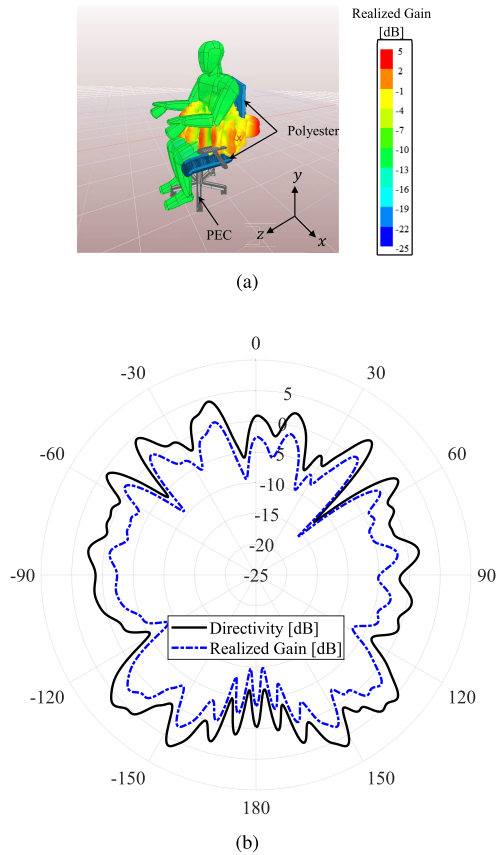
(a)

(b)

FIGURE 16. Simulated results of the antenna's performance while the patient is sitting on the chair with a polyester cover and the corresponding parameters of $\varepsilon_{pol} = 3.2$, $\mu_{pol} = 1$, $tan\delta_{pol} = 0.03$; a) 3-D radiation pattern and b) E-plane ($X - Z$ plane) patterns at the frequency of 5.8 GHz.
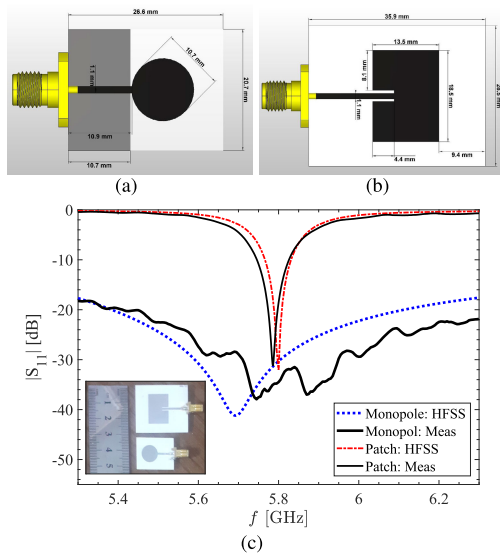

(a)   (b)

(c)

FIGURE 17. a, b) Geometry and dimensions of the monopole and patch antennas based on RO4003 with $\varepsilon_r = 3.55$, $H = 0.508$ mm, and $tan\delta = 0.0027$, and c) simulated and measured input reflection coefficient versus frequency.

designed based on RO4003 with $\varepsilon_r = 3.55$, $H = 0.508$ mm, and $tan\delta = 0.0027$. Besides, Fig. 17(c) indicates a close
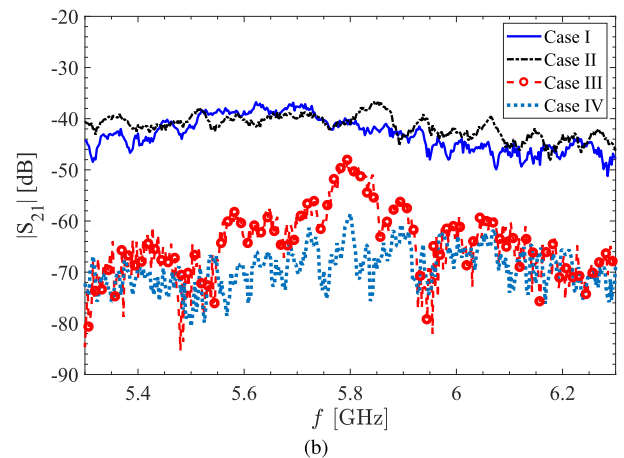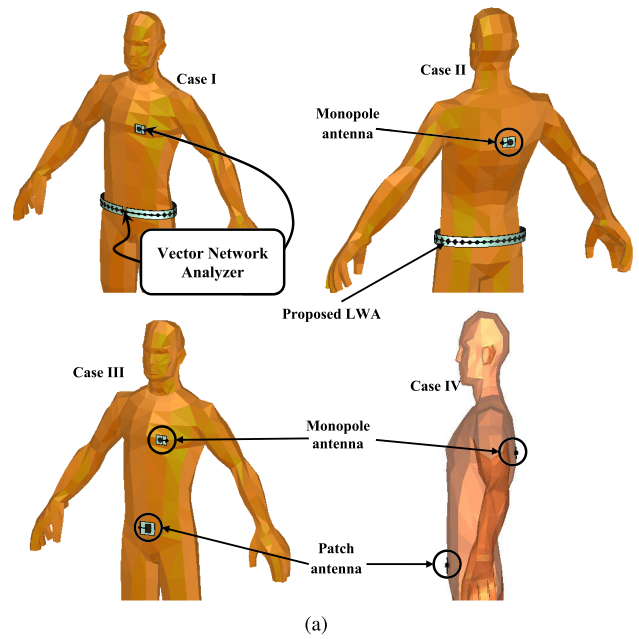

(a)

(b)

FIGURE 18. Measuring transmission coefficient between the sensor and hub including a) geometry of four different cases, b) measured S_{21} results, where, Case I) monopole antenna as a sensor on the chest and the proposed LWA as the hub, Case II) monopole antenna as a sensor on the back and the proposed LWA as the hub, Case III) monopole antenna as a sensor on the chest and the patch antenna as the hub, and Case IV) monopole antenna as a sensor on the back and the patch antenna as the hub.

agreement between simulation and measurement results of the input reflection coefficient $|S_{11}|$.

In Fig. 18(a), four measurement cases are shown to evaluate the path loss in on-body communication links, of which results are illustrated in Fig. 18(b). In Case I, the proposed LWA is bent around the body's abdomen and the monopole antenna is stuck on the chest, in front of the heart. To measure the path loss, a vector network analyzer (HP) is utilized so that both network's ports are connected to the antennas. It should be noted that the noise level of the network is approximately below -80 dB. For the Case I, the measurement result is $|S_{2,1}| \approx -40$ dB at the frequency of 5.8 GHz. Similarly, in Case II, the sensor is placed on the back. Clearly, the

TABLE 3. Comparison of the antenna performance between the proposed work and published literature.

Ref.	Size $[\lambda_0^2]$	Substrate; ε_r	f [GHz]	$S_{11} < -10$ dB Bandwidth	Measured Gain [dBi]	Pattern shape	Pol	SAR_{1g} [W/kg]
[16]	0.318×0.318	RT5880; 2.2	2.45	7.7%	2	Uni	L	1.15
[17]	0.18×0.18	FR4; 4.4	2.38	2.8%	-5.4	Omni	L	0.74
			5.8	9%	2.7	Uni	C	0.85
[18]	0.64×0.64	RT5880; 2.2	2.4	5%	0.2	Omni	L	0.2
			5.8	40.7%	4.3	Uni		0.1
[20]	0.27×0.37	RT5870; 2.33	2.45	1.2%	2.1	Uni	L	–
			5.8	1.9%	5.1			
[21]	0.81×1.45	Foam; 1.2	5.8	3.9%	3.1	Uni	L	–
[24]	0.31×0.31	FR4; 4.4	2.44	3.3%	6.3	Uni	L	0.29
[25]	0.41×0.41	PDMS; 2.8	2.44	15.9%	5.2	Uni	C	0.18
[26]	1×1	Ro3850; 2.9	3.5	23.6%	9.4	Uni	L	0.07
		Ro3003; 3	5.8	14%	6.6			0.33
Proposed LWA	18.56×0.97	Ro4003; 3.55	5.8	7%	2	Quasi-omni	L	0.015

Uni and Omni represent unidirectional and omnidirectional patterns, respectively. SAR values are renormalized to 0.1W input power. L and C denote linear and circular polarizations, respectively.
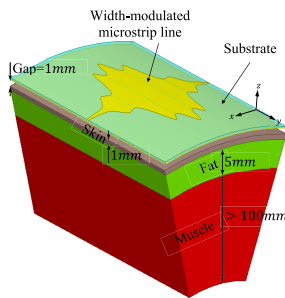

FIGURE 19. The cross-section view of the three-layer tissue model including skin, fat, and muscle.

FIGURE 20. Simulation of 3-D SAR_{1g} distribution with 1 W input power of the proposed LWA at 5.8 GHz.

TABLE 4. Material properties of the human tissue model at 5.8 GHz [56].

	Skin	Fat	Muscle
ε_r	35.11	4.95	48.48
σ (S/m)	3.71	0.29	4.96
ρ (kg/m^3)	1090	930	1050

measurement result for this case is similar to that of Case I. In fact, there is a rather small variation in path loss by moving the sensor around the body. As seen from Fig. 18(b) in Cases III and IV, the designed microstrip patch antenna is used similar to existing hubs on the body's abdomen. As expected, the path loss in Case III is less than that of IV (i.e., $|S_{2,1}|_{CaseIII} > |S_{2,1}|_{CaseIV}$) because the distance between the sensor and hub in Case III is closer than in Case IV. Based on the provided information in Fig. 18(b), the on-body communication link in the proposed LWA clearly outperforms conventional antennas. As expected, if a patient lies on the ground or in bed, the proposed LWA will not be blocked and the continuous communication link between sensors and antenna will be established.

C. EVALUATION OF SPECIFIC ABSORPTION RATE (SAR)

As discussed in previous sections, the designed antenna should be worn as a belt around the abdomen of the human body. Therefore, it is needed to evaluate the performance of the implemented LWA with an adjacency of the phantom model. Fig. 19 shows the cross-section view of the
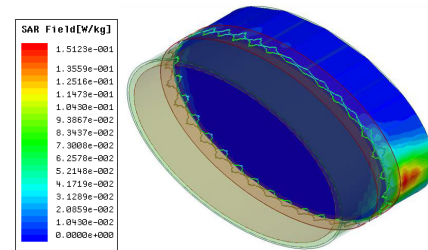
phantom model, which has an elliptical shape, with three layers including skin, fat, and muscle. It should be noted that the gap spacing between the antenna and the phantom model is about 1 mm. Moreover, the dielectric properties of the human tissue model at 5.8 GHz are listed in Table 4. For safety considerations, the maximum radiation absorbed by the human body should be lower than 1.6 W/kg over 1 g of the tissue [37]. Fig. 20 depicts the 3-D SAR distribution of the designed LWA at 5.8 GHz. The obtained maximum SAR value is about 0.15 W/kg corresponding to the 1 W input power, which satisfies the corresponding SAR_{1g} limitation in the IEEE C95 standard for WBANs [29]. Furthermore, the obtained maximum SAR values at the frequencies of 5.725 and 5.875 GHz are about 0.179 and 0.144 W/kg, respectively.

D. COMPARATIVE ANALYSIS

For completeness, a fair comparison between the proposed LWA and other antenna designs in previous literature is provided in Table 3. Comparison criteria include size, substrate type, design frequency, matching bandwidth, realized gain, pattern type, antenna's input power, maximum SAR level, and polarization type. It is worth mentioning that the majority of antenna types in previous works are designed in either monopole or patch forms, while the proposed antenna is designed based on a leaky-wave structure. In fact, existing antennas radiate based on resonance elements, while the radiation in this work is occurred relying on the leakage

phenomenon. According to Table 3, the maximum SAR value of the proposed antenna is significantly smaller than that of other works. As a benchmark for 100 mW input power, the simulated maximum SAR value of the proposed LWA is about 0.015 W/kg.

VI. CONCLUSION

In this paper, a practical IoMT-based WBAN has been investigated where the health monitoring of patients could be continuously performed, without any interruption or data collision. Accordingly, an orthogonal coding was used for on-body communications and a heuristic antenna was designed for the hub, to manage off-body link communications. Therefore, a specific antenna with an omnidirectional pattern in the azimuth plane is required with an acceptable SAR value. In this regard, a periodic conformal LWA based on a width-modulated microstrip line with eliminated the 2nd stopband was proposed as a result of which a quasi-omnidirectional pattern was provided at the dedicated WBAN ISM frequency of 5.8 GHz. Since the radiation occurs through the leakage phenomenon, the presented antenna showed a wide impedance bandwidth whilst the WBAN ISM band [5.725–5.875] GHz was completely supported. The designed conformal LWA is flexible enough such that it can be bent similar to a belt around the human body-abdomen. Simulated and measured radiation patterns had an omnidirectional behavior with ripples about 3 and 3.5 dBi in the azimuth $(X-Z)$ plane, respectively. The simulated and measured half-power beam-widths were about 68° and 72° in the vertical $(Y-Z)$ plane, respectively. With on-body communication links (i.e., the connection between hub and sensors), measurement results depict that the path loss of the link between sensors and the proposed antenna is considerably smaller than that of sensors and conventional hub antennas. For an input power of 1 W, simulation results of the maximum SAR level over 1 g of the tissue was about 0.15 W/kg which confirms that this antenna will not break the IEEE SAR limits.

APPENDIX A
THEORETICAL CONSIDERATIONS IN MODULATED DIELECTRIC MEDIA

As described in previous literature [48], [49] for TM mode, the magnetic filed component for a modulated dielectric medium in Eq. (8) can be represented as follows:

$$H_y(z) = \sum_{n=-\infty}^{\infty} C_n \sqrt{\varepsilon_{e_r}} e^{-jk_{z_n}z}, \quad (10)$$

where $k_{z_n} = \kappa + \frac{2n\pi}{d}$ and C_n are unknown coefficients to be determined by applying boundary conditions. Using an innovative method described in [57], the fundamental wavenumber κ can simply be obtained as:

$$\sin^2\left(\frac{\kappa d}{2}\right) = \Delta(0) \sin^2\left(\frac{\pi \sqrt{\theta_0}}{2}\right), \quad (11)$$

in which $\Delta(0)$ denotes the determinant of the known matrix $[B_{mn}]$ whose elements are

$$B_{mn} = \begin{cases} \dfrac{\theta_{m-n}}{\theta_0 - (2m)^2} & m \neq n \\ 1 & m = n, \end{cases} \quad (12)$$

where θ_m depends on k_0, d, M_n, and ε_{avg}. As an example, for a sinusoidally modulated dielectric medium (where $M_n = 0$, $\forall\, n \geq 2$), θ_m may be expanded as

$$\theta_0 = \left(\frac{k_0 d}{\pi}\right)^2 \varepsilon_{avg} + 1 - \frac{1}{\sqrt{1 - M_1^2}}, \quad (13a)$$

$$\theta_1 = \frac{M_1}{2}\left(\frac{k_0 d}{\pi}\right)^2 \varepsilon_{avg} + \frac{4b^3 - 2b}{b^2 - 1}, \quad (13b)$$

$$\theta_n = \frac{(3n+1)b^{n+2} - (3n-1)b^n}{b^2 - 1}, \quad (\forall\, n \geq 2), \quad (13c)$$

$$b = \frac{1}{M_1}\left(\sqrt{1 - M_1^2} - 1\right). \quad (13d)$$

For modulated dielectric media with a multi-tone periodicity where $\theta_m \neq 0$ at least 2 numbers of m, θ_m can be numerically calculated. Besides, having found κ, the phase constant of all space harmonics for such a periodic medium can be easily achieved.

REFERENCES

[1] L. Sun, X. Jiang, H. Ren, and Y. Guo, "Edge-cloud computing and artificial intelligence in Internet of Medical Things: Architecture, technology and application," *IEEE Access*, vol. 8, pp. 101079–101092, 2020.

[2] L. Mucchi, S. Jayousi, S. Caputo, E. Paoletti, P. Zoppi, S. Geli, and P. Dioniso, "How 6G technology can change the future wireless health-care," in *Proc. 2nd 6G Wireless Summit (6G SUMMIT)*, Mar. 2020, pp. 1–6.

[3] K. Wei, L. Zhang, Y. Guo, and X. Jiang, "Health monitoring based on Internet of Medical Things: Architecture, enabling technologies, and applications," *IEEE Access*, vol. 8, pp. 27468–27478, 2020.

[4] S. Gopikrishnan, P. Priakanth, G. Srivastava, and G. Fortino, "EWPS: Emergency data communication in the Internet of Medical Things," *IEEE Internet Things J.*, vol. 8, no. 14, pp. 11345–11356, Jul. 2021.

[5] Z. Askari, J. Abouei, M. Jaseemuddin, A. Anpalagan, and K. N. Plataniotis, "A Q-learning approach for real-time NOMA scheduling of medical data in UAV-aided WBANs," *IEEE Access*, vol. 10, pp. 115074–115091, 2022.

[6] *IEEE Standards for Local and Metropolitan Area Networks—Part 15.6: Wireless Body Area Networks*, Standard 802.15.6-2012, IEEE Standards Association, Feb. 2012.

[7] D. P. Tobón, T. H. Falk, and M. Maier, "Context awareness in WBANs: A survey on medical and non-medical applications," *IEEE Wireless Commun.*, vol. 20, no. 4, pp. 30–37, Aug. 2013.

[8] M. N. Suma, P. C. Bybi, and P. Mohanan, "A wideband printed monopole antenna for 2.4-GHz WLAN applications," *Microw. Opt. Technol. Lett.*, vol. 48, no. 5, pp. 871–873, May 2006.

[9] D. Yang, J. Hu, and S. Liu, "A low profile UWB antenna for WBAN applications," *IEEE Access*, vol. 6, pp. 25214–25219, 2018.

[10] U. Illahi, J. Iqbal, M. I. Sulaiman, M. M. Alam, M. M. Su'Ud, M. H. Jamaluddin, and M. N. M. Yasin, "Design of new circularly polarized wearable dielectric resonator antenna for off-body communication in WBAN applications," *IEEE Access*, vol. 7, pp. 150573–150582, 2019.

[11] S. N. Mahmood, A. J. Ishak, A. Ismail, A. C. Soh, Z. Zakaria, and S. Alani, "ON-OFF body ultra-wideband (UWB) antenna for wireless body area networks (WBAN): A review," *IEEE Access*, vol. 8, pp. 150844–150863, 2020.

[12] Y. I. Nechayev, P. S. Hall, and Z. H. Hu, "Characterisation of narrowband communication channels on the human body at 2.45 GHz," *IET Microw., Antennas Propag.*, vol. 4, no. 6, pp. 722–732, Jun. 2010.

[13] S. Yan, P. J. Soh, and G. A. E. Vandenbosch, "Wearable ultrawideband technology—A review of ultrawideband antennas, propagation channels, and applications in wireless body area networks," *IEEE Access*, vol. 6, pp. 42177–42185, 2018.

[14] A. Iqbal, A. Smida, A. J. Alazemi, M. I. Waly, N. K. Mallat, and S. Kim, "Wideband circularly polarized MIMO antenna for high data wearable biotelemetric devices," *IEEE Access*, vol. 8, pp. 17935–17944, 2020.

[15] Q. Bai and R. Langley, "Crumpling of PIFA textile antenna," *IEEE Trans. Antennas Propag.*, vol. 60, no. 1, pp. 63–70, Jan. 2012.

[16] A. Arif, M. Zubair, M. Ali, M. U. Khan, and M. Q. Mehmood, "A compact, low-profile fractal antenna for wearable on-body WBAN applications," *IEEE Antennas Wireless Propag. Lett.*, vol. 18, no. 5, pp. 981–985, May 2019.

[17] X.-Q. Zhu, Y.-X. Guo, and W. Wu, "Miniaturized dual-band and dual-polarized antenna for MBAN applications," *IEEE Trans. Antennas Propag.*, vol. 64, no. 7, pp. 2805–2814, Apr. 2016.

[18] H. Xiaomu, S. Yan, and G. A. E. Vandenbosch, "Wearable button antenna for dual-band WLAN applications with combined on and off-body radiation patterns," *IEEE Trans. Antennas Propag.*, vol. 65, no. 3, pp. 1384–1387, Mar. 2017.

[19] W. Su, J. Zhu, H. Liao, and M. M. Tentzeris, "Wearable antennas for cross-body communication and human activity recognition," *IEEE Access*, vol. 8, pp. 58575–58584, 2020.

[20] X. Zhu, Y. Guo, and W. Wu, "A compact dual-band antenna for wireless body-area network applications," *IEEE Antennas Wireless Propag. Lett.*, vol. 15, pp. 98–101, 2016.

[21] Y. Hong, J. Tak, and J. Choi, "An all-textile SIW cavity-backed circular ring-slot antenna for WBAN applications," *IEEE Antennas Wireless Propag. Lett.*, vol. 15, pp. 1995–1999, 2016.

[22] M. Särestöniemi, C. Pomalaza-Ráez, C. Kissi, M. Berg, M. Hämäläinen, and J. Iinatti, "WBAN channel characteristics between capsule endoscope and receiving directive UWB on-body antennas," *IEEE Access*, vol. 8, pp. 55953–55968, 2020.

[23] B. Wang and S. Yan, "Design of smartwatch integrated antenna with polarization diversity," *IEEE Access*, vol. 8, pp. 123440–123448, 2020.

[24] Y.-S. Chen and T.-Y. Ku, "A low-profile wearable antenna using a miniature high impedance surface for smartwatch applications," *IEEE Antennas Wireless Propag. Lett.*, vol. 15, pp. 1144–1147, 2016.

[25] Z. H. Jiang, Z. Cui, T. Yue, Y. Zhu, and D. H. Werner, "Compact, highly efficient, and fully flexible circularly polarized antenna enabled by silver nanowires for wireless body-area networks," *IEEE Trans. Biomed. Circuits Syst.*, vol. 11, no. 4, pp. 920–932, Aug. 2017.

[26] M. El Atrash, M. A. Abdalla, and H. M. Elhennawy, "A wearable dual-band low profile high gain low SAR antenna AMC-backed for WBAN applications," *IEEE Trans. Antennas Propag.*, vol. 67, no. 10, pp. 6378–6388, Oct. 2019.

[27] A. Y. I. Ashyap, S. H. B. Dahlan, Z. Z. Abidin, M. I. Abbasi, M. R. Kamarudin, H. A. Majid, M. H. Dahri, M. H. Jamaluddin, and A. Alomainy, "An overview of electromagnetic band-gap integrated wearable antennas," *IEEE Access*, vol. 8, pp. 7641–7658, 2020.

[28] A. A. Oliner, D. R. Jackson, and J. Volakis, "Leaky-wave antennas," in *Antenna Engineering Handbook*, vol. 4. New York, NY, USA: McGraw-Hill, 2007, ch. 4, pp. 1–56.

[29] Y. B. Li, X. Wan, B. G. Cai, Q. Cheng, and T. J. Cui, "Frequency-controls of electromagnetic multi-beam scanning by metasurfaces," *Sci. Rep.*, vol. 4, no. 1, p. 6921, Nov. 2014.

[30] N. Montaseri and A. Mallahzadeh, "One-dimensional leaky-wave antenna with scanning through the broadside based on sinusoidally modulated reactance surface," *IET Microw., Antennas Propag.*, vol. 13, no. 2, pp. 190–196, Feb. 2019.

[31] N. Montaseri and A. Mallahzadeh, "Modulated reactance surfaces with several modulation indices for multibeam leaky-wave antenna design," *IEEE Trans. Antennas Propag.*, vol. 68, no. 12, pp. 8156–8161, Dec. 2020.

[32] A. M. Hakimi, A. Keivaan, H. Oraizi, and A. Amini, "Wide-scanning circularly polarized reflector-based modulated metasurface antenna enabled by a broadband polarizer," *IEEE Trans. Antennas Propag.*, vol. 70, no. 1, pp. 84–96, Jan. 2022.

[33] Z. Peng, W. Yang, S. Shi, M. Jiang, J. Gao, and G. Zhai, "High scanning rate asymmetrical dual-beam leaky wave antenna using sinusoidally modulated reactance superposing surface," *IEEE Trans. Antennas Propag.*, vol. 70, no. 12, pp. 12258–12263, Dec. 2022.

[34] S. Ramalingam, C. A. Balanis, C. R. Birtcher, S. Pandi, and H. N. Shaman, "Axially modulated cylindrical metasurface leaky-wave antennas," *IEEE Antennas Wireless Propag. Lett.*, vol. 17, no. 1, pp. 130–133, Jan. 2018.

[35] K. J. Nicholson, T. C. Baum, and K. Ghorbani, "Conformal Voronoi metasurface antenna embedded in a composite structural laminate," *IEEE Trans. Antennas Propag.*, vol. 69, no. 7, pp. 3717–3725, Jul. 2021.

[36] J. Abouei, "A set of cyclic orthogonal codes acquired from Walsh–Hadamard matrix," in *Proc. 34th Int. Math. Conf.*, Shahrood, Iran, Sep. 2003, pp. 1–4.

[37] *IEEE Standard for Safety Levels With Respect to Human Exposure to Radio Frequency Electromagnetic Fields, 3 KHz to 300 GHz*, Standard IEEE C95. 1-1991, IEEE Standards Coordinating Committee, Apr. 1992.

[38] T. Yuan, N. Yuan, and L.-W. Li, "A novel series-fed taper antenna array design," *IEEE Antennas Wireless Propag. Lett.*, vol. 7, pp. 362–365, 2008.

[39] H. Yi, L. Li, J. Han, and Y. Shi, "Traveling-wave series-fed patch array antenna using novel reflection-canceling elements for flexible beam," *IEEE Access*, vol. 7, pp. 111466–111476, 2019.

[40] B. G. P. Shariff, T. Ali, P. R. Mane, and P. Kumar, "Array antennas for mmWave applications: A comprehensive review," *IEEE Access*, vol. 10, pp. 126728–126766, 2022.

[41] D. W. Boeringer and D. H. Werner, "Particle swarm optimization versus genetic algorithms for phased array synthesis," *IEEE Trans. Antennas Propag.*, vol. 52, no. 3, pp. 771–779, Apr. 2004.

[42] D. G. Kurup, M. Himdi, and A. Rydberg, "Synthesis of uniform amplitude unequally spaced antenna arrays using the differential evolution algorithm," *IEEE Trans. Antennas Propag.*, vol. 51, no. 9, pp. 2210–2217, Sep. 2003.

[43] S. Paulotto, P. Baccarelli, F. Frezza, and D. R. Jackson, "A novel technique for open-stopband suppression in 1-D periodic printed leaky-wave antennas," *IEEE Trans. Antennas Propag.*, vol. 57, no. 7, pp. 1894–1906, Jul. 2009.

[44] S. Otto, A. Al-Bassam, A. Rennings, K. Solbach, and C. Caloz, "Transversal asymmetry in periodic leaky-wave antennas for bloch impedance and radiation efficiency equalization through broadside," *IEEE Trans. Antennas Propag.*, vol. 62, no. 10, pp. 5037–5054, Oct. 2014.

[45] J. T. Williams, P. Baccarelli, S. Paulotto, and D. R. Jackson, "1-D combline leaky-wave antenna with the open-stopband suppressed: Design considerations and comparisons with measurements," *IEEE Trans. Antennas Propag.*, vol. 61, no. 9, pp. 4484–4492, Sep. 2013.

[46] R. Ranjan and J. Ghosh, "SIW-based leaky-wave antenna supporting wide range of beam scanning through broadside," *IEEE Antennas Wireless Propag. Lett.*, vol. 18, no. 4, pp. 606–610, Apr. 2019.

[47] M. Guglielmi and D. R. Jackson, "Broadside radiation from periodic leaky-wave antennas," *IEEE Trans. Antennas Propag.*, vol. 41, no. 1, pp. 31–37, Jan. 1993.

[48] N. Montaseri and A. Mallahzadeh, "Broadside radiation in leaky-wave antenna using multiperiodic width-modulated microstrip lines," *IEEE Antennas Wireless Propag. Lett.*, vol. 18, no. 1, pp. 207–211, Dec. 2019.

[49] C. Yeh, K. F. Casey, and Z. A. Kaprielian, "Transverse magnetic wave propagation in sinusoidally stratified dielectric media," *IEEE Trans. Microw. Theory Techn.*, vol. MTT-13, no. 3, pp. 297–302, May 1965.

[50] T. Tamir, H. C. Wang, and A. A. Oliner, "Wave propagation in sinusoidally stratified dielectric media," *IEEE Trans. Microw. Theory Techn.*, vol. MTT-12, no. 3, pp. 323–335, May 1964.

[51] L. Matekovits and T. S. Bird, "Width-modulated microstrip-line based mantle cloaks for thin single- and multiple cylinders," *IEEE Trans. Antennas Propag.*, vol. 62, no. 5, pp. 2606–2615, Feb. 2014.

[52] M. V. Kuznetcov, V. G. Buendía, Z. Shafiq, L. Matekovits, D. E. Anagnostou, and S. K. Podilchak, "Printed leaky-wave antenna with aperture control using width-modulated microstrip lines and TM surface-wave feeding by SIW technology," *IEEE Antennas Wireless Propag. Lett.*, vol. 18, no. 9, pp. 1809–1813, Sep. 2019.

[53] M. Kobayashi, "A dispersion formula satisfying recent requirements in microstrip CAD," *IEEE Trans. Microw. Theory Techn.*, vol. 36, no. 8, pp. 1246–1250, Aug. 1988.

[54] G. A. Conway and W. G. Scanlon, "Antennas for over-body-surface communication at 2.45 GHz," *IEEE Trans. Antennas Propag.*, vol. 57, no. 4, pp. 844–855, Apr. 2009.

[55] R. Negra, I. Jemili, and A. Belghith, "Wireless body area networks: Applications and technologies," *Proc. Comput. Sci.*, vol. 83, pp. 1274–1281, Jan. 2016.

[56] C. Gabriel, "Compilation of the dielectric properties of body tissues at RF and microwave frequencies," Final Rep., Jun. 1996.

[57] P. M. Morse and H. Feshbach, "Methods of theoretical physics," *Amer. J. Phys.*, vol. 22, no. 6, pp. 410–413, Sep. 1954.

NASSER MONTASERI received the M.Sc. degree in electrical engineering from the Iran University of Science and Technology (IUST), Tehran, Iran, in 2012, and the Ph.D. degree in electrical engineering from Shahed University, Tehran, in 2019. He is currently a Researcher with the Iran Telecommunication Research Center (ITRC). His current research interests include metasurfaces, metamaterials, phased-array antennas, reconfigurable antennas, leaky-wave antennas, and guided waves along periodic and complex media.
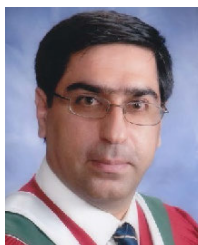
ZEYNAB KHODKAR received the B.Sc. degree in electrical engineering, from Shariaty Technical University, Tehran, Iran, in 2009, and the M.Sc. degree in electrical engineering from Shiraz Azad University, Shiraz, Iran, in 2013. Since 2021, she has been with the Delta Innovation Center, Iran University of Science and Technology, Tehran, to research and develop wireless communication systems. Her research interests include the physical layer of wireless communication systems, next-generation cellular networks, massive MIMO, cognitive radio, information theory, and related areas.

JAMSHID ABOUEI (Senior Member, IEEE) received the B.Sc. degree in electronics engineering and the M.Sc. degree in communication systems engineering from the Isfahan University of Technology, Iran, in 1993 and 1996, respectively, and the Ph.D. degree in electrical engineering from the University of Waterloo, Canada, in 2009. He joined as a Lecturer with the Department of Electrical Engineering, Yazd University, Iran, in 1996, and was promoted to Assistant Professor, in 2010, and Associate Professor, in 2015. From 2009 to 2010, he was a Postdoctoral Fellow with the Department of Electrical and Computer Engineering, University of Toronto, Canada. During his sabbatical, he was an Associate Researcher with the Department of Electrical, Computer and Biomedical Engineering, Ryerson University, Canada. His research interests include 5G and wireless sensor networks (WSNs), with a particular emphasis on PHY/MAC layer designs, including the energy efficiency and optimal resource allocation in cognitive cell-free massive MIMO networks, multiuser information theory, mobile edge computing, and femtocaching.

WILLIAM G. WHITTOW (Senior Member, IEEE) received the B.Sc. degree in physics and the Ph.D. degree in computational electromagnetics from The University of Sheffield, Sheffield, U.K., in 2000 and 2004, respectively. From 2004 to 2012, he was a Research Associate with Loughborough University, Loughborough, U.K. In 2012, he became a Lecturer with the Wolfson School of Mechanical, Electrical and Manufacturing Engineering (WSMEME), Loughborough University. He became a Senior Lecturer, in 2014, a Reader (Associate Professor), in 2018, and a Professor of radiofrequency materials, in 2020. He currently leads the Wireless Communications Research Group (WiCR) and is the Director of the Connected Infrastructure Research Hub. He is a named Investigator on research grants totaling more than £12 million. He has authored more than 250 peer-reviewed journals and conference papers on topics related to metamaterials, metasurfaces, synthetic and heterogeneous dielectrics, dielectric measurements, 3D-printing, wearable antennas and phantoms, specific absorption rate, embroidered antennas, inkjet printing, and RFID tags. He is the inaugural male Associate Fellow of WES and a Senior Fellow of the Higher Education Academy. In 2017, he received the Women in Engineering Society (WES) Men as Allies Award. From 2007 to 2011, he was the Coordinating Chair of the Loughborough Antennas and Propagation Conference (LAPC). He has served as an Associate Editor for *IET Electronics Letters* and *IET Microwaves, Antennas and Propagation*. He serves on the technical program committees for several IEEE international conferences. He has been asked to give more than 25 invited conference presentations and a four-day invited workshop on bioelectromagnetics and teaches about dielectric measurements with the European School of Antennas. More than 90 of his academic journal articles can be freely downloaded here:
http://publications.lboro.ac.uk/publications/all/collated/elwgw.html

KONSTANTINOS (KOSTAS) N. PLATANIOTIS (Fellow, IEEE) received the B.Eng. degree in computer engineering from the University of Patras, Greece, and the M.S. and Ph.D. degrees in electrical engineering from the Florida Institute of Technology, Melbourne, FL, USA.

He has been holding the Bell Canada Endowed Chair in Multimedia, since 2014. He is currently a Professor with the Edward S. Rogers Sr. Department of Electrical and Computer Engineering, University of Toronto, Toronto, ON, Canada, where he directs the Multimedia Laboratory. His research interests include image/signal processing, machine learning, adaptive learning systems, visual data analysis, multimedia and knowledge media, and affective computing. He is a Fellow of the Engineering Institute of Canada and the Canadian Academy of Engineering. He was the Technical Co-Chair of the IEEE 2013 International Conference on Acoustics, Speech and Signal Processing. He served as the Inaugural IEEE Signal Processing Society Vice President for Membership (2014–2016) and the General Co-Chair for the 2017 IEEE GLOBALSIP. He served as the General Co-Chair for the 2018 IEEE International Conference on Image Processing (ICIP 2018) and the IEEE International Acoustics, Speech and Signal Processing (ICASSP 2021). He will be the General Chair for the 2027 IEEE International Conference on Acoustics, Speech and Signal Processing (ICASSP 2027), Toronto. He has served as the Editor-in-Chief for the IEEE SIGNAL PROCESSING LETTERS. He is a registered Professional Engineer in the province of Ontario.

• • •